Multistream instabilities in three-species plasmas formed around strong double layers

V. Lapuerta and E. Ahedo
E.T.S.I. Aeronáuticos, Universidad Politécnica de Madrid, 28040 Madrid, Spain

(Received 11 March 2002; accepted 15 May 2002)

An electron–electron–ion (e-e-i) and an ion–ion–electron (i-i-e) plasma are formed on the sides of a strong double layer. A detailed parametric investigation of the linear dispersion relation of these three-species plasmas is carried out in order to determine the different current-driven instabilities that can form in each of them. Both the electron–electron (e-e) and the ion–electron (i-e) instabilities develop in the e-e-i plasma. The first one dominates over practically its whole domain of existence and presents up to five different types. The second one involves the three plasma species and differs from the classical two-species version: it is resistive for most parametric ranges, with the reactive type occupying only a small parametric region within the high-drift range. Either two i-e instabilities or one i-e and one ion–ion instability can develop simultaneously in the i-i-e plasma, depending on the ratio of the velocities of the two beams involved. For both types of plasmas, different forms of branch mixing between the two unstable modes are identified. © *2002 American Institute of Physics.* [DOI: 10.1063/1.1492285]

I. INTRODUCTION

Intermediate strong double layers (DL) are typical of small Debye-length plasmas formed in some electrical discharges, natural auroras, triple plasma chambers, and plasma contactors (operating in the electron-collecting mode).[1–4] A strong DL is a non-neutral sheath characterized by a potential jump much larger than the temperatures of the two quasineutral plasmas on its sides. In the quasineutral scale of these two plasmas, the DL can be considered a free surface discontinuity, which accelerates one plasma species from each side and confines the two remaining ones, as Fig. 1 illustrates. Two different three-species plasmas are formed at each side. At the high-potential side, there is an electron–electron–ion (e-e-i) plasma consisting of a population of confined electrons (c), a high-velocity beam of electrons (e) emerging from the DL, and a population of ions (i) moving toward the DL. Similarly, at the low-potential side of the DL, there is an ion–ion–electron (i-i-e) plasma constituted by the high-velocity i beam emerging from the DL, the population e moving toward the DL, and a population a of confined ions. Ahedo *et al.* presented a steady spherical model of the whole structure (DL plus the two plasmas) for an electron-collecting plasma contactor.[5]

Experiments show that DL structures are stable in time, but, in general, present high levels of fluctuations of different frequencies on both sides of the DL.[2,3] The high-velocity beams created by the DL make current-driven instabilities the most plausible cause of the fluctuations. However there is controversy on which is the dominant instability, and there is no detailed study of the influence of the different plasma parameters. Numerical simulations of particular DL structures detected an electron–electron (e-e) instability in the high potential side and an ion–electron (i-e) instability in the low potential side, but these simulations could not stabilize the DL structure.[6] The gentle-bump instability (a limit case of the e–e instability) has been suggested to explain the anomalous heating observed in experiments with electron-collecting plasma contactors.[7] Several theoretical works on plasma contactor plumes[8–10] proposed the simultaneous development, on the high-potential side, of the Buneman and ion-acoustic instabilities, two limit cases of the i-e instability, but these proposals are based mainly on extrapolating classical results from two-species plasmas. In fact, a recent perturbation analysis of the steady spherical model of Ref. 5 concluded that a reactive i-e instability (which includes the Buneman type) did not develop.[11]

Early work on current-driven instabilities in multispecies plasmas was done by Stringer, who, for a particular case of a four-species plasma, determined the parametric regions of existence of e-e, i-e, and ion–ion (i-i) instabilities.[12] Electron–electron–ion plasmas have been studied numerically by Gary, but for parametric ranges unusual in DL configurations.[13,14] In a plasma with no net electrical current, he detected the cold-beam, gentle-bump, ion-acoustic, and Buneman instabilities; in another case, with net electrical current, he found the electron-acoustic instability. References 15 and 16 studied the characteristics of ion-acoustic waves in ion–ion–electron plasmas but treated damped modes only.

This paper attempts to elucidate which stream instabilities develop and dominate on each DL side by analyzing directly the dispersion relation of both e-e-i and i-i-e plasmas. The exact dispersion relation for a homogeneous, infinite plasma constituted by drifting Maxwellian species can be expressed as[17]

$$1+\sum_{\alpha}\frac{\omega_{p\alpha}^2}{k^2c_\alpha^2\gamma_\alpha-(\omega-kV_\alpha)^2}=0, \tag{1}$$

with

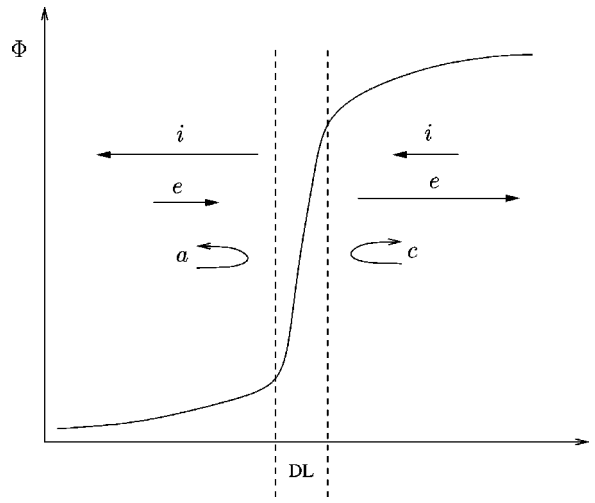

FIG. 1. Sketch of a typical axial profile of the electrostatic potential in a plasma structure with an intermediate DL. The potential jump at the DL accelerates the populations *i* of ions and *e* of electrons. At the high potential side, the fast *e* beam interacts with the slow *i* beam and the population *c* of confined electrons. At the low potential side, the fast *i* beam interacts with the slow *e* beam and the population *a* of confined ions. For $\lambda_D \to 0$ the DL reduces to a discontinuity and the plasmas on both sides are quasineutral.

$$\gamma_\alpha \equiv \gamma(z_\alpha) = z_\alpha^2 + \frac{1}{R(z_\alpha)}, \quad z_\alpha = \frac{\omega - kV_\alpha}{kc_\alpha}. \tag{2}$$

Here k and ω are the (real) wave number and (complex) frequency, respectively, of a linear plasma perturbation, and, for each species α, $\omega_{p\alpha} = \sqrt{e^2 n_\alpha / \epsilon_0 m_\alpha}$ is the natural frequency (based in the species density n_α), $c_\alpha \equiv \sqrt{T_\alpha / m_\alpha}$ is the thermal velocity (based in the species temperature T_α), V_α is the macroscopic velocity, z_α is the relative phase velocity of the wave, γ_α is the complex pressure-to-density linear response function, and $R(z) \equiv R_1(z) + \mathrm{i}\, R_2(z)$, with

$$R_1(z) = 1 - z \exp(-z^2/2) \int_0^z \exp(y^2/2) dy,$$

$$R_2(z) = \sqrt{\pi/2} z \exp(-z^2/2), \tag{3}$$

is the plasma dispersion function.[18] Plots and asymptotic expressions of the complex functions $\gamma(z)$ and $R(z)$, for z real, can be found in Ref. 17. We recall that the use of $\gamma(z)$ in Eq. (1) allows one a unified analysis of both resistive (i.e., based in Landau resonance effects) and reactive instabilities.

For a three-species plasma, the solutions $\omega(k)$ of Eq. (1) depend on five dimensionless parameters, yielding too many different situations for a single discussion. This paper is centered in ranges of parameters adequate to plasma conditions around strong DLs, although other ranges are treated, when interesting conclusions can be made out of them. The e-e-i plasma is discussed in Sec. II and the i-i-e plasma in Sec. III.

Throughout the paper we will use the results of a recent general parametric study of the two-stream instability.[19] There, we determined the parametric regions of dominance of the different acoustic, Langmuir, and reactive types of the two-stream instability, and we derived analytical expressions of the maximum growth rate for all types, and of the velocity threshold for the less unstable types.

II. INSTABILITY MODES IN AN E-E-I PLASMA

The plasma at the high-potential side of a DL consists of a quiescent electron population (c), an electron beam (e) of velocity V_e, and an ion beam (i) of velocity V_i. Making use of the quasineutrality condition

$$n_i \simeq n_e + n_c, \tag{4}$$

the dispersion relation for this plasma depends on five dimensionless parameters: n_e/n_c, V_e/c_e, T_e/T_c, V_i/c_e, and T_i/T_c. For the DL case, the two last parameters are generally small and have a secondary role in the stability behavior. Hence, most of the discussion here is restricted to the limits $V_i/c_e, T_i/T_c \to 0$. For each set of parameters, the characteristics (k, ω) of the most unstable mode will be represented with an asterisk as superscript (ω_{im}^*, k^*, etcetera).

Starting from the long-wavelength case, $k\lambda_{D\alpha} \to 0$, and for the three main parameters of order unity, the solutions of Eq. (1) for the e-e-i plasma are in three different frequency ranges.

(i) At $\omega \sim \omega_p = \sqrt{\omega_{pc}^2 + \omega_{pe}^2}$, there is one pair of Langmuir waves following

$$\omega \simeq kV_e \frac{n_e}{n_i} \pm \omega_p \left[1 + \frac{k^2}{2\omega_p^2} \left(\frac{n_c}{n_i} \gamma_c c_c^2 + \frac{n_e}{n_i} \gamma_e c_e^2 \right) \right]. \tag{5}$$

(ii) At $\omega \sim kV_e$, there is one pair of e-e acoustic waves satisfying

$$\frac{\omega}{k} \simeq V_e \frac{n_c}{n_i} \pm \left(\frac{n_e \gamma_c c_c^2 + n_c \gamma_e c_e^2}{n_i} - \frac{n_e n_c}{n_i^2} V_e^2 \right)^{1/2}. \tag{6}$$

(iii) At $\omega \sim kV_e \sqrt{m_e/m_i}$, there is one pair of i-e acoustic waves following

$$\frac{\omega}{k} \simeq \left(\frac{m_e}{m_i} \frac{n_i \gamma_c c_c^2 (\gamma_e c_e^2 - V_e^2)}{n_c (\gamma_e c_e^2 - V_e^2) + n_e \gamma_c c_c^2} \right)^{1/2}. \tag{7}$$

Several related observations are of interest here. First, ions remain quasirigid for the high-frequency (Langmuir and e-e) modes, while the electron response is quasisteady for the i-e modes. Second, each pair of high-frequency modes is mounted on a reference frame moving with an intermediate speed between those of the two electron populations. Third, the values of $\gamma_c = \gamma(z_c)$ and $\gamma_e = \gamma(z_e)$ are different for the three pairs of modes: one can take

$$\gamma_c = \gamma_e = \gamma(\infty) = 3$$

for the Langmuir waves, Eq. (5),

$$\gamma_c \simeq \gamma(0) = 1, \quad \gamma_e \simeq \gamma(-V_e/c_e) \tag{8}$$

for the i-e waves, Eq. (7), but z_c and z_e depend on ω/k for the e-e waves, leaving Eq. (6) an implicit equation for ω/k. Four, since the imaginary component of γ_α is nonzero except for $z_\alpha = 0$ and $z_\alpha = \infty$, unstable solutions for the i-e and e-e modes are very likely. This will be confirmed by the compu-

TABLE I. Characteristics of the different types of the e-e instability for $T_e/T_c \ll n_e/n_c$. Results have been obtained by making species $a=c$, $b=e$ in Ref. 19.

Type	Approximate domain	$\omega_{im}^*/\omega_{pc}$
CB	$1 \ll \frac{V_e}{c_c}$	$\frac{\sqrt{3}}{2^{4/3}}\left(\frac{n_e}{n_c}\right)^{1/3}$
SA	$\frac{V_e}{c_c}=O(1)$	$O\left(\frac{n_e}{n_c}\right)^{1/2}$
WA	$\frac{n_e}{n_c} \ll \left(\frac{V_e}{c_c}\right)^2 \ll 1$	$\sqrt{\frac{\pi}{54}}\frac{V_e}{c_c}\left(\frac{n_e}{n_c}\right)^{1/2}$
WL	$\left(\frac{V_e}{c_c}\right)^2 \ll \frac{n_e}{n_c}$	$\frac{\sqrt{2\pi}}{27}\left(\frac{V_e}{c_c}\right)^3\left(\frac{n_c}{n_e}\right)^{1/2}$

tation of the exact solution of Eq. (1), but first we discuss independently the main properties of the e-e and i-e instabilities for an e-e-i plasma.

A. The electron–electron instability

At the high-frequency range of the e-e modes, the ions remain frozen in their equilibrium solution and only two electron populations contribute to Eq. (1). Our general parametric analysis of the two-stream instability demonstrates that the e-e instability can take five different types depending on n_e/n_c, V_e/c_e, and T_e/T_c. Tables I and II summarize the approximate domains and the respective maximum growth rates of the different types for all possible situations (notice that the roles of the e and c populations can be exchanged and it is enough to consider the interval $n_e/n_c \leqslant 1$). In Tables I and II, CB stands for cold beam, SL for strong Langmuir, WL for weak Langmuir, SA for strong acoustic, and WA for weak acoustic. The gentle-bump instability[20] corresponds to the SL instability, and the electron-acoustic instability[14] covers both the WL and WA instability domains.[19] Detailed expressions for the instability threshold of the WA, WL, and SL instabilities can be found in Ref. 19. Figures 2(a) and 2(b) depict the exact threshold of the e-e instability, and the approximate domains of the different types for $n_e/n_c=10^{-3}$ (weak-beam case) and $n_e/n_c=1$ (strong-beam case), respectively. As the density ratio moves from the weak-beam to the strong-beam case, we observe that (i) the instability threshold does not changes much, and (ii) the weak-Langmuir instability tends to occupy the whole domains of the acoustic and strong-Langmuir instabilities.

TABLE II. Characteristics of the different types of the e-e instability for $n_e/n_c \ll T_e/T_c$. Results have been obtained by making species $a=e$, $b=c$ in Ref. 19.

Type	Approximate domain	$\omega_{im}^*/\omega_{pc}$
CB	$\frac{T_e}{T_c}\left(\frac{n_c}{n_e}\right)^{2/3} \ll \left(\frac{V_e}{c_c}\right)^2$	$\frac{\sqrt{3}}{2^{4/3}}\left(\frac{n_e}{n_c}\right)^{1/3}$
SL	$\frac{T_e}{T_c} \ll \left(\frac{V_e}{c_c}\right)^2 \ll \frac{T_e}{T_c}\left(\frac{n_c}{n_e}\right)^{2/3}$	$\sqrt{\frac{\pi}{8\mathrm{e}}}\frac{n_e}{n_c}\left(\frac{V_e}{c_e}\right)^2$
WL	$\left(\frac{V_e}{c_c}\right)^2 \ll \frac{T_e}{T_c}$	$\frac{\sqrt{2\pi}}{27}\left(\frac{V_e}{c_e}\right)^3\left(\frac{n_e}{n_c}\right)^{1/2}$

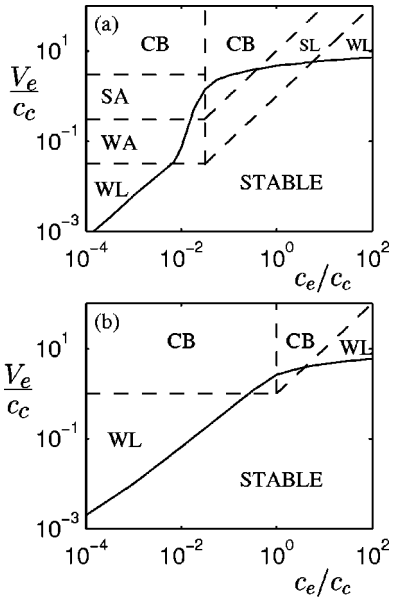

FIG. 2. Parametric regions of existence of the different types of the e-e instability for (a) $n_e/n_c=10^{-3}$ and (b) $n_e/n_c=1$. The solid lines represent the instability threshold.

B. The ion–electron instability

The most important types of the i-e instability in an e-e-i plasma are going to be the acoustic ones. These are characterized by a quasisteady response of the two-electron populations. Dropping inertia effects for electrons in Eq. (1) and using Eq. (8), the i-e acoustic modes satisfy (for $V_i \ll V_e$)

$$\left(\frac{\omega}{k}-V_i\right)^2-\gamma_i c_i^2=\frac{c_s^2}{k^2\lambda_{De}^2+S(V_e/c_e,\Lambda_{ec})-\mathrm{i}\ R_2(V_e/c_e)}, \tag{9}$$

with

$$\Lambda_{ec}=\frac{\lambda_{De}}{\lambda_{Dc}}\equiv\sqrt{\frac{n_c T_e}{n_e T_c}},\quad c_s=c_e\sqrt{\frac{m_e}{m_i}}, \tag{10}$$

and

$$S(V_e/c_e,\Lambda_{ec})=R_1(V_e/c_e)+\Lambda_{ec}^2. \tag{11}$$

Equation (9) extends Eq. (7) to $k\lambda_{De}\geqslant O(1)$, and generalizes to an e-e-i plasma ($\Lambda_{ec}\neq 0$) the expression of the acoustic i-e instability in a two-species plasmas [Eq. (13) in Ref. 19].

Extending the reasoning of Ref. 17 to the denominator of Eq. (9), the character of the i-e instability depends on the value of $|R_2/S|$ and the sign of the function S. The first ratio measures the effects of Landau resonance of the population e (for species c we have $\gamma_c=1$). The sign of S distinguishes between resistive and reactive responses: the i-e modes are purely resistive for $S>0$, whereas reactive effects compete with Landau resonance for $S<0$. For $\Lambda_{ec}=0$, one has $S<0$ for $V_e/c_e>1.31$, but the region with reactive effects shrinks as Λ_{ec} increases. Since the minimum of function R_1

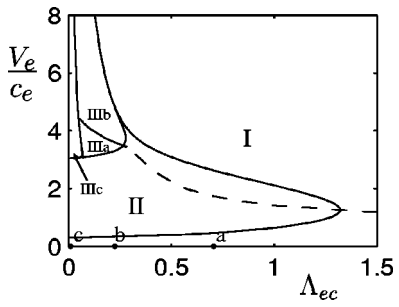

FIG. 3. Parametric regions of the different types of the i-e instability in an e-e-i plasma. Regions I, II, and III correspond approximately to the WA, SA, and reactive instabilities, respectively. Subregions IIIa, IIIb, and IIIc, representing different reactive responses, are for $T_e/T_c=1$ and $m_e/m_i=10^{-4}$. The dashed line is the locus of the maximum of the function $\omega_{im}^*(V_e)$, obtained from Eq. (9). Black points a, b, and c refer to Figs. 4(a)–4(c).

is -0.28, reactive effects disappear totally for an e-e-i plasma with $\Lambda_{ec}^2>0.28$. This is the first major difference with the case $\Lambda_{ec}=0$.

Figure 3 sketches the approximate regions of the different types of the i-e instability in an e-e-i plasma. Region I, characterized by $|R_2/S|\ll 1$ and $S>0$, corresponds to a weak-acoustic instability. Region II, characterized by $|R_2/S|\gtrsim O(1)$, corresponds to a strong-acoustic instability; notice that the line $S=0$ is inside region II, so that for $S<0$ reactive effects start to compete with the (dominant) Landau resonance effects. Regions III, characterized by $|R_2/S|\to 0$ and $S<0$, correspond to a purely reactive instability. For $V_e/c_e\gg 1$, the boundary of regions III is at

$$V_e/c_e\simeq\Lambda_{ec}^{-1}. \tag{12}$$

We observe that the WA and SA i-e instabilities occupy the *whole* range of drift velocities for $\Lambda_{ec}>0.29$, approximately.

The approximate equation (9) is applicable to the two acoustic types. The wave response for the SA case must be determined numerically. On the contrary, the WA instability follows the asymptotic expressions

$$\frac{\omega_{re}}{k}\simeq V_i\pm\frac{c_s}{(k^2\lambda_{De}^2+S)^{1/2}},\quad \frac{\omega_{im}}{k}\simeq\pm\frac{c_s}{2}\frac{R_2(V_e/c_e)}{(k^2\lambda_{De}^2+S)^{3/2}} \tag{13}$$

(for $T_i/T_e\to 0$), where from the most unstable mode satisfies

$$\frac{\omega_{im}^*}{\omega_{pi}}\simeq\sqrt{\frac{n_e}{n_i}}\frac{R_2(V_e/c_e)}{3^{3/2}S},\quad k^*\lambda_{De}=\sqrt{\frac{S}{2}}. \tag{14}$$

These expressions generalize to $\Lambda_{ec}\neq 0$ the classical ones for the ion-acoustic instability.[20] Notice that Eqs. (13) and (14) take different simplified forms for (i) $V_e/c_e\ll 1$, (ii) $V_e/c_e\gg 1$, and (iii) $V_e/c_e=O(1)$ and $\Lambda_{ec}\gg 1$.

Although ignored in the preceding discussion, the WA i-e instability becomes a weak-Langmuir instability within the thin region $V_e/c_s\lesssim O[(1+\Lambda_{ec}^2)^{-1}]$. For such low drifts, electron inertia is not negligible and the maximum growth rate follows,[19]

$$\frac{\omega_{im}^*}{\omega_{pi}}\simeq\sqrt{\frac{n_e}{n_i}}\frac{1}{3}\sqrt{\frac{\pi}{6}}\frac{1}{1+\Lambda_{ec}^2}\frac{V_e}{c_e},\quad k^*\lambda_{De}\simeq\sqrt{\frac{1+\Lambda_{ec}^2}{2}}. \tag{15}$$

A second major difference of the present i-e instability (and a consequence of the previous one) is that, for Λ_{ec} nonzero and constant, the strongest unstable mode [that is, the one with $\omega_{im}^*(V_e)$ maximum] is not found at $V_e/c_e\to\infty$ but an intermediate drift velocity. Within the acoustic regions, that maximum is close to the maximum of $|R_2/S|$, at $V_e/c_e\sim\Lambda_{ec}^{-1}$. The dashed line in Fig. 3 plots the exact position of the maximum. The physical reason to find the most unstable mode at an intermediate drift velocity lies in the c population having an stabilizing role. The importance of the c population increases with n_c/n_e, but, in addition, perturbations on n_c tend to dominate over those on n_e for V_e/c_e large.

The third relevant difference is related to the behavior of the reactive instability in region III. First, Ref. 17 showed that Eq. (9) is not valid when Landau resonance effects become negligible, because it overestimates ω_{im}^*. Small electron inertia effects turn out to be the mechanism bounding the maximum growth rate. The novelty in an e-e-i plasma is that three different situations arise, as Fig. 3 illustrates. In the marginal subregion IIIc, characterized by

$$1\ll V_e/c_e\ll\Lambda_{ec}^{-1}(\omega_{pi}/\omega_{pe})^{1/3},$$

a classical Buneman instability with

$$\frac{\omega_{im}^*}{\omega_{pe}}\simeq\frac{\sqrt{3}}{2^{4/3}}\left(\frac{m_e}{m_i}\frac{n_i}{n_e}\right)^{1/3} \tag{16}$$

is found. In subregion IIIa, a reactive instability, with $\gamma_e\simeq 3$, $\gamma_c\simeq 1$, develops, but no simple expressions for $\omega(k)$ are available. In subregion IIIb, the preceding reactive instability practically disappears due to the interaction with the e-e instability. The threshold of the e-e instability separates regions IIIa and IIIb. The following explains better the interaction between the two instability modes in region IIIb.

C. Exact solution and mode interaction

We consider now the exact solution of the dispersion relation (1) and the interaction between the i-e and e-e instabilities. For T_e/T_c and n_e/n_c fixed, the dispersion relation yields two lines $\omega_{im}^*(V_e)$, one for the i-e instability and one for the e-e instability. Three distinguished types of interaction between these lines are found depending on the value of n_e/n_c. Figures 4(a) to 4(c) plot the three types for $T_e/T_c=1$. These are as follows.

Case (a): $0<n_e/n_c\lesssim O(1)$, Fig. 4(a). The e-e instability is dominant within, practically, its whole domain of existence. A resistive i-e instability exists outside that domain, and there is no trace of the reactive instability. The interaction between the i-e and e-e instabilities, when they exist simultaneously, is weak. The maximum of the i-e instability line is to the left of the e-e instability threshold; it increases and moves toward larger drift velocities as n_e/n_c increases. The transition to case (b) happens when the position of that maximum reaches the vicinity of the threshold of the e-e instability.

Case (b): $1\ll n_e/n_c\ll m_i/m_e$, Fig. 4(b). The situation is similar to case (a) except that the i-e and e-e branches interact strongly at drift velocities close to the threshold of the e-e

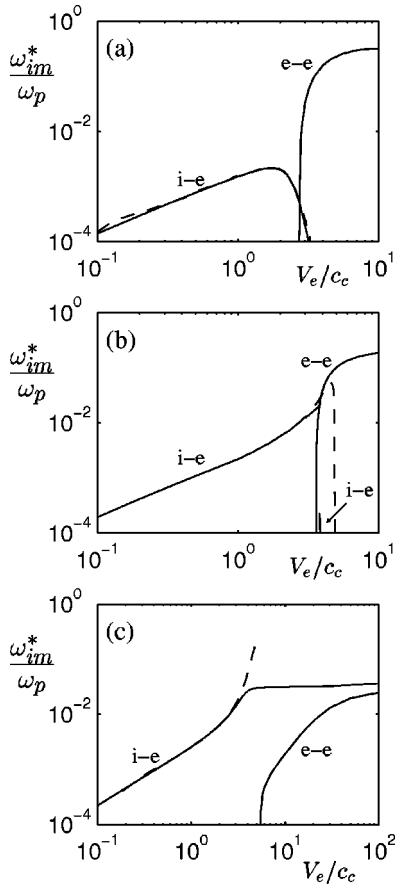

FIG. 4. An e-e-i plasma: Evolution of $\omega^*_{im}(V_e)$ of the i-e and e-e instabilities, for $n_e/n_c=2$(a), 20(b), and 15000 (c). Other parameters are $T_e/T_c=1$ and $m_e/m_i=10^{-4}$. The dashed lines correspond to the solutions of the quasisteady approximation, Eq. (9), for the i-e instability; the good agreement of this approximation for the acoustic regions can be observed.

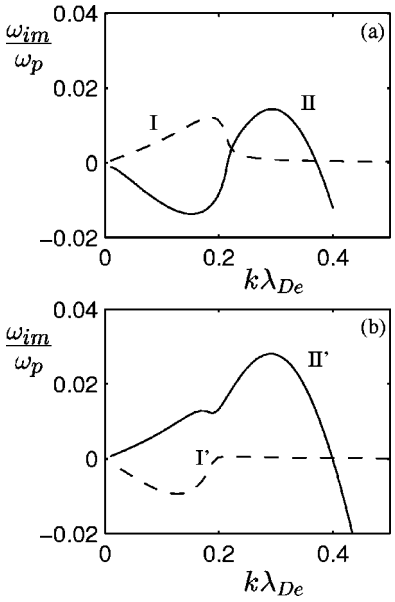

FIG. 5. An e-e-i plasma: Evolution of $\omega_{im}(k)$ for (a) $V_e/c_c=3.75$(a) and 3.79(b), before and after the branch mixing. Other parameters as in Fig. 4(b).

instability. As a consequence, the i-e instability line decays sharply above that threshold. The strong interaction is due to a mixing of the branches $\omega(k)$ carrying the two instabilities; mathematically, branch mixing is a double root of the dispersion relation (1). Figures 5(a) and 5(b) illustrate the topological changes in the $\omega(k)$ response of the two unstable modes around the point of branch mixing: in Fig. 5(a), branch I is the i-e mode and branch II is the e-e mode (just above the threshold of the e-e instability); Fig. 5(b) shows the situation after the mixing, with branch II′ carrying the above-mentioned two unstable modes, and branch I′ presenting a tiny maximum, corresponding to the residual i-e instability depicted in Fig. 4(b). For $T_e/T_c=1$, we can place the transition between cases (a) and (b) at $n_e/n_c\simeq 5.9$, where branch mixing starts to happen. As n_e/n_c continues increasing, the maximum of the e-e instability moves to larger drift velocities and decreases. The transition to case (c) takes place when the maxima of the e-e and i-e instabilities are similar.

Case (c): $m_i/m_e \ll n_e/n_c$, Fig. 4(c). This is a marginal case where the i-e instability dominates in the whole velocity range. For an e-e-i plasma with $T_e/T_c \gtrsim O(1)$, this is the only density range where a Buneman-type instability is found at $V_e/c_e \gg 1$.

Figures 4(a)–4(c) are for $T_e/T_c=1$ and there are some significant changes when $T_e/T_c \ll 1$. In order to show them, Figs. 6(a) and 6(b) depict the lines $\omega^*_{im}(V_e)$ for $n_e/n_c=0.05$ and two disparate temperature ratios. Figure 6(a) is simply the continuation of Fig. 4(a) for a lower n_e/n_c. Figure 6(b) corresponds to the case (b) of strong interaction. Comparing it to Fig. 4(b), we observe that (i) a reactive i-e instability develops now; and (ii) the e-e instability line does not depart from the threshold case $\omega^*_{im}=0$. This last aspect is the consequence of a branch mixing different from that of Figs. 5(a) and 5(b). Figures 7(a)–7(c) illustrate the new branch mixing: for $V_e/c_c=10^{-2}$, only the i-e instability exists; at $V_e/c_c\simeq 0.075$ a second maximum appears in the only

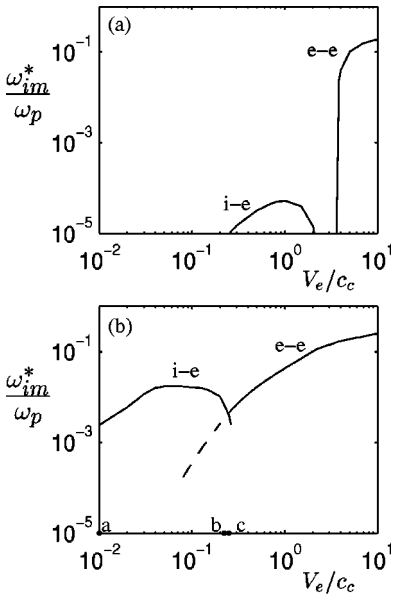

FIG. 6. An e-e-i plasma: Evolution of $\omega^*_{im}(V_e)$ of the i-e and e-e instabilities, for $T_e/T_c=1$(a) and 10^{-4}(b). Other parameters are $n_e/n_c=0.05$ and $m_e/m_i=10^{-4}$. Black points a, b, and c refer to Figs. 7(a)–7(c).

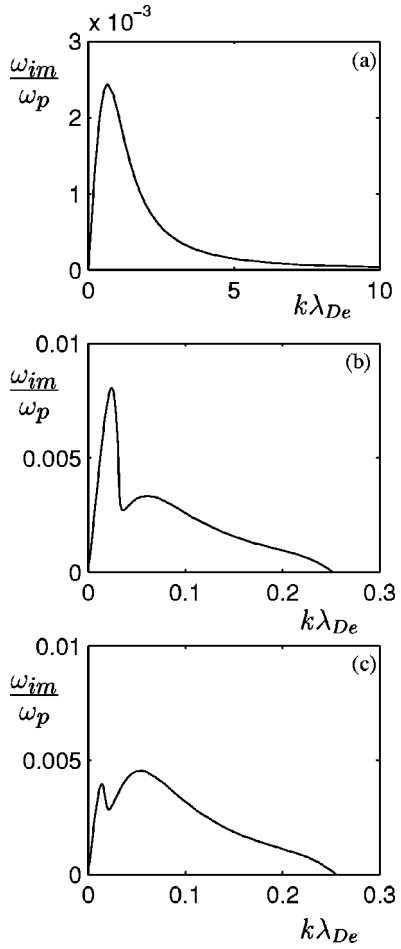

FIG. 7. An e-e-i plasma: Evolution of $\omega_{im}(k)$ for $V_e/c_c=10^{-2}$(a), 0.22(b), and 0.25(c). Other parameters as in Fig. 6(b).

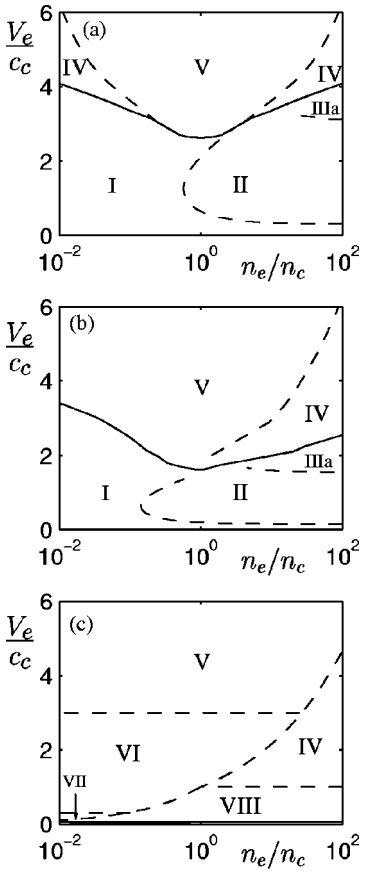

FIG. 8. An e-e-i plasma: Approximate regions of dominance of different i-e and e-e stability types for $T_e/T_c=1$(a), 0.25(b), and 10^{-4}(c). Region I stands for WA i-e, region II for SA i-e, region III for reactive i-e, region IV for SL e-e, region V for CB e-e, region VI for SA e-e, region VII for WA e-e, and region VIII for WL e-e. The solid line is the e-e instability threshold.

unstable $\omega(k)$ branch; this second maximum becomes dominant at $V_e/c_c\simeq 0.25$ and the only one at $V_e/c_c\simeq 0.27$, taking then the characteristics of an e-e mode.

The range $T_e/T_c\gg 1$ does not present further novelties and it is unusual in double-layer configurations. A numerical study of the case $T_e/T_c=100$, $n_e/n_c=1$, and $0\leqslant V_e/c_c\leqslant 20$ was done by Gary,[14] who found an e-e acoustic instability [indeed, a WL instability according to Fig. 2] whereas the i-e modes were stable.

Figures 8(a)–8(c) summarize the influence of the three parameters n_e/n_c, V_e/c_c, and T_e/T_c on the regions of dominance of the different e-e and i-e instability types. The solid lines are the threshold of the e-e instability and bound roughly the region of dominance of this instability. Regions I to IIIa correspond to the i-e instability of Fig. 3. The reactive region is rather small in all cases: for $T_e/T_c=O(1)$ because it is placed around n_e/n_c large; and for $T_e/T_c\ll 1$ because the e-e instability dominates in practically the whole velocity range. Notice that the e-e-i plasma at the high potential side of a DL has n_e/n_c small;[5] the present analysis justifies more in detail the absence of the reactive i-e instability in the plasma-plus-DL structure, as we found recently.[11] Finally, notice that Fig. 8 corresponds to a zero ion temperature, when the threshold of the i-e instability is at $V_e/c_e=0$. That threshold increases with T_i/T_e, and it is placed at $V_e/c_e\sim 1$ for $T_i/T_e\sim 1$, the reduction thus affecting region I mainly.

Regions IV–VIII represent the different types of the e-e instability. For $T_e/T_c=O(1)$, the cold-beam region V covers most of the e-e instability domain. The rest of the e-e domain, region IV, belong to a strong Langmuir instability; as T_e/T_c decreases the SL instability is more likely found for n_e/n_c large. The five types of the e-e instability are present for $T_e/T_c\ll 1$, Fig. 8(c). It is worth noting the large region VI of the strong-acoustic e-e instability, not reported previously, whereas the e-e acoustic instability (WL and WA instabilities) covers the small regions VII and VIII.

III. INSTABILITY MODES IN AN I-I-E PLASMA

The i-i-e plasma of the low potential side of a double layer consists of a quiescent population of ions (a), a beam of electrons (e) of velocity V_e, and a beam of ions (i) of velocity V_i; the i and e beams are counterstreaming, with $V_e>0$ and $V_i<0$. Making use of the quasineutrality condition

$$n_e=n_i+n_a, \tag{17}$$

the eigenmodes of the dispersion relation (1) depend now on the five parameters n_i/n_e, V_e/c_e, V_i/c_i, T_a/T_e, and T_i/T_e.

For the large wavelength limit, $k\lambda_{D\alpha}\to 0$, and the distinguished limits

$$V_e/c_e \gg O(1), \quad V_i, V_e\sqrt{m_e/m_i} \gg O(c_i), O(c_a), \tag{18}$$

the eigenmodes of Eq. (1) are: (i) one pair of (high-frequency) Langmuir modes, mounted on the e-beam, with $\omega\sim\omega_{pe}$, satisfying

$$\omega \simeq kV_e \pm \omega_{pe}\left[1+\frac{\gamma_e k^2}{2\omega_{pe}^2}c_e^2\right], \tag{19}$$

with $\gamma_e\simeq 3$; and (ii)–(iii) two pairs of low-frequency modes with frequencies in the ranges $\omega\sim kV_i$ and $\omega\sim kV_e\sqrt{m_e/m_i}$. The characteristic types of these low-frequency modes depend on the ratio

$$\mu_{ei}=\left|\frac{V_e}{V_i}\sqrt{\frac{m_e}{m_i}}\right| \equiv \left|\frac{V_e/c_e}{V_i/c_s}\right|,$$

between the beam velocities; c_s was defined in Eq. (10). First, for $\mu_{ei}\ll 1$, there are two pairs of i-e modes satisfying

$$\frac{\omega}{k}\simeq V_i \pm \left(\gamma_i c_i^2+\frac{n_i}{n_e}\frac{m_e}{m_i}(\gamma_e c_e^2 - V_e^2)\right)^{1/2}, \tag{20}$$

$$\frac{\omega}{k}\simeq \pm\left(\gamma_a c_a^2+\frac{n_a}{n_e}\frac{m_e}{m_i}(\gamma_e c_e^2 - V_e^2)\right)^{1/2}. \tag{21}$$

Physically, the ''slow'' e beam sees two ion populations with very different velocities and interacts separately with them, producing two pairs of i-e modes. These are similar to the classical i-e modes in a two-species plasma *except for* the density ratios, n_i/n_e and n_a/n_e, involved in Eqs. (20) and (21). In the opposite range, $\mu_{ei}\gg 1$, there is one pair of i-e modes following

$$\frac{\omega}{k}\simeq \pm\left(\frac{m_e}{m_i}(\gamma_e c_e^2 - V_e^2)\right)^{1/2}, \tag{22}$$

and one pair of i-i modes satisfying

$$\frac{\omega}{k}=\frac{n_a}{n_e}V_i \pm \left(\frac{n_a\gamma_i c_i^2 + n_i\gamma_a c_a^2}{n_e}-\frac{n_i n_a}{n_e^2}V_i^2\right)^{1/2}. \tag{23}$$

Now, the ''fast'' e beam sees the two ion populations as a single one, and the interaction yields the classical pair of i-e modes. The i-i pair of modes, of lower frequency, corresponds to the residual interaction between the two ion populations.

For $V_e/c_e\ll O(1)$ and any μ_{ei}, the electron response is quasisteady in the low-frequency modes and we can take $\gamma_e\simeq\gamma(-V_e/c_e)$. If, in addition, we consider the distinguished case $T_i, T_a \ll T_e$, Eqs. (20)–(23) become explicit on ω/k and predict the existence of either two i-e instabilities or one i-e and one i-i instability, depending on the value of μ_{ei}. This is confirmed by the exact solution. Figures 9(a) and 9(b) show the evolution of the maximum growth rate of the two unstable modes with V_e/c_e, for two values of V_i/c_s, and for T_i/T_e, $T_a/T_e\to 0$. The black points on the horizontal axis mark the transition case $\mu_{ei}=1$. For μ_{ei} small the two ion-electron instabilities, i-e and a-e, can be observed, whereas

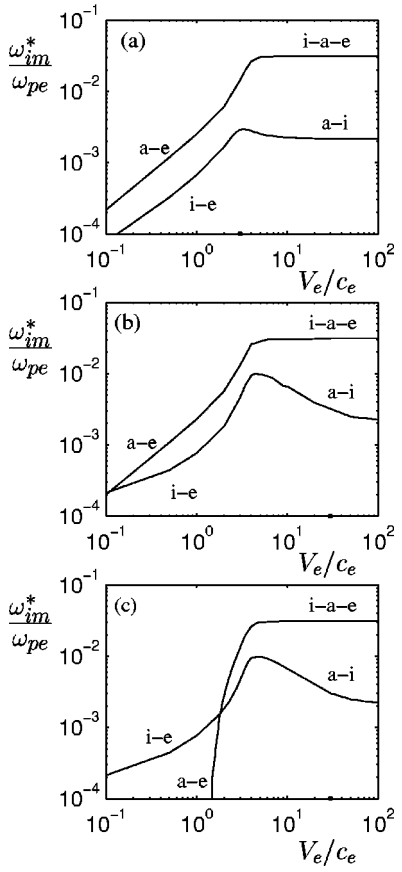

FIG. 9. An i-i-e plasma: Evolution of $\omega^*_{im}(V_e)$ for: (a) $V_i/c_s=-3$ and $T_a/T_e=0$; (b) $V_i/c_s=-30$ and $T_a/T_e=0$; (c) $V_i/c_s=-30$ and $T_a/T_e=1$. Other parameters: $n_i/n_e=0.2$, $T_i/T_e=0$, and $m_e/m_i=10^{-4}$. Black points correspond to $\mu_{ei}=1$.

for μ_{ei} large i-a-e represents the ion-electron instability (which involves now the three species) and a-i represents the ion–ion instability.

Asymptotic expressions of ω^*_{im} for $\mu_{ei}\ll 1$ and the i-e mode are

$$\frac{\omega^*_{im}}{\omega_{pi}}\simeq\frac{\sqrt{2\pi}}{27}\sqrt{\frac{m_e}{m_i}}\frac{n_e}{n_i}\frac{|V_e-V_i|^3}{c_s^3} \tag{24}$$

for $|V_e-V_i|\ll c_s\sqrt{n_i/n_e}$ (a WL instability),

$$\frac{\omega^*_{im}}{\omega_{pi}}\simeq\sqrt{\frac{\pi}{54}}\sqrt{\frac{m_e}{m_i}}\frac{|V_e-V_i|}{c_s} \tag{25}$$

for $c_s\sqrt{n_i/n_e}\ll|V_e-V_i|\ll c_e$ (a WA instability), and Eq. (16) for $c_e\ll|V_e-V_i|$ (a CB instability). Expressions for the a-e instability are obtained by changing subscript i to subscript a in these formulas. As Figs. 9(a) and 9(b) illustrate, the dominant instability mode depends on V_e/c_e, n_i/n_a, and $|1-V_i/V_e|$. For nonzero ion temperatures, the velocity threshold of the i-e and a-e instabilities increase with the respective temperature ratio, T_i/T_e and T_a/T_e. Figures 9(b) and 9(c) illustrate this point for T_a/T_e.

For μ_{ei} large, the ion–ion (here $i-a$) instability behaves like a two-stream instability, since the perturbation of the electron beam are very small and can be dropped from the dispersion relation. A paradoxical conclusion is that the i-i

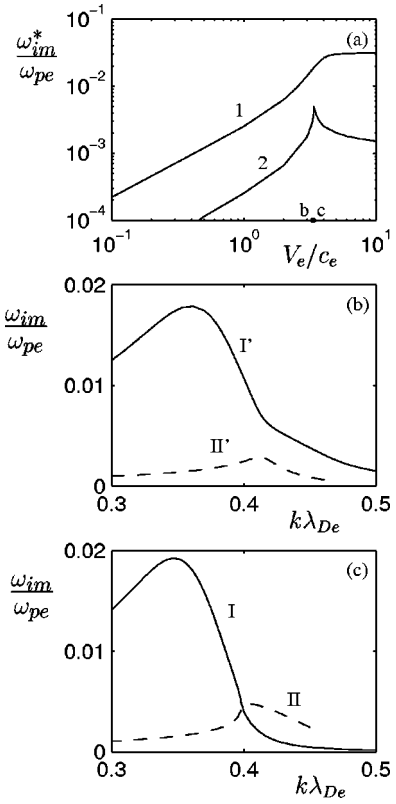

FIG. 10. An i-i-e plasma: In (a), $\omega_{im}^*(V_e)$ for $V_i/c_s=5$, $n_i/n_e=0.01$, $T_i=T_a=0$, and $m_e/m_i=10^{-4}$; the black points correspond to the two next plots. In (b) and (c), $\omega_{im}(k)$ for $V_e/c_e=3.3$(a) and 3.4(b), before and after the branch mixing.

instability has the same wave response than the e-e instability, in spite of the disparate frequency range and ''opposite'' behavior of the ''third'' species: whereas the ion population remains quasifrozen in the high-frequency e-e modes, the electron beam responds quasisteadily in the low-frequency i-i modes, *but* with very small perturbations. Neglecting electron perturbations, ω_{im}^* for the *i-a* instability is independent of V_e/c_e, and is maximum in the cold beam limit, $V_i/c_s\to\infty$. Then it satisfies

$$\frac{\omega_{im}^*}{\omega_{pe}}\simeq\frac{1}{2^{3/2}}\sqrt{\frac{m_e}{m_i}}, \tag{26}$$

for the strong-beam case, $n_i/n_a=1$, and

$$\frac{\omega_{im}^*}{\omega_{pe}}\simeq\frac{3^{1/2}}{2^{4/3}}\sqrt{\frac{m_e}{m_i}}\left(\frac{n_a}{n_e}\right)^{1/6}\left(\frac{n_i}{n_e}\right)^{1/3} \tag{27}$$

for the weak-beam case, $n_i/n_a\ll 1$. Asymptotic expressions of ω_{im}^* for the *i-a-e* instability and $\mu_{ei}\gg 1$ are obtained by exchanging n_i/n_e to 1 and neglecting V_i in Eqs. (24)–(25) and (16). The *i-a-e* instability dominates always over the *a-i* instability.

Branch mixing (i.e., a double root of the dispersion relation) has been detected only for cases when the *i* and *e* beams are not counterstreaming (which is not the case in the DL configuration). Figure 10(a) shows an example with branch mixing coinciding with the sharp peak of curve 2. Figures 10(b) and 10(c) plot the two branches $\omega_{im}(k)$ at the vicinity of the the double root. It is worth noting that this mixing is different from the two previous ones, shown in Figs. 5 and 7: here each branch carries one maximum of $\omega_{im}(k)$ before and after the mixing.

Finally, we write down the exact explicit expression of ω/k of the four low-frequency modes for the particular case $n_i=n_a$, $c_i, c_a\to 0$, and quasisteady electrons:

$$\left(\frac{\omega}{k}-\frac{V_i}{2}\right)^2=\frac{V_i^2}{4}+\frac{c_s^2}{2(k^2\lambda_{De}^2+R(-V_e/c_e))}\pm\left(\frac{V_i^2}{2}\frac{c_s^2}{k^2\lambda_{De}^2+R(-V_e/c_e)}+\frac{c_s^4}{4[k^2\lambda_{De}^2+R(-V_e/c_e)]^2}\right)^{1/2}.$$

This expression, just like Eq. (9), shows that the resistive or reactive character of the two instabilities depends basically on the sign of $R_1(V_e/c_e)$, that is on V_e/c_e being smaller or larger than 1.31.

IV. CONCLUSIONS

We have investigated the current-driven instabilities that develop in e-e-i and i-i-e plasmas, with special (but not exclusive) attention to the parametric conditions of the plasmas formed around strong double layers.

For e-e-i plasmas (with an electron population at rest) the following conclusions are reached.

(i) Both an e-e and e-i instabilities develop. The ion population never interacts independently with the two electron species and two i-e instabilities cannot develop simultaneously (as some previous works postulated).

(ii) The e-e instability dominates within most of its domain of existence. For $T_e/T_c=O(1)$, it is mainly of the cold-beam type, but for $T_e/T_c\ll 1$ up to five different types develop in different parametric ranges.

(iii) The i-e instability always involves the interaction of the ions with the two electron populations and presents relevant novelties with respect to the classical two-species one. The main one is that a (weak or strong) acoustic i-e instability develops not only for low drift velocities but for most of the high drift range.

(iv) The most unstable i-e mode corresponds to an intermediate value of the drift velocity, where the unstable effect of the Landau resonance of population *e* is maximum. In addition, the stabilizing effect of population *c* tends to dominate at high drifts.

(v) The parametric region of the reactive i-e instability is further reduced by the overlapping with the region of existence of the e-e instability. The interaction of the two unstable modes results in a sharp decay of the i-e instability. A Buneman i-e instability is found only for a marginal parametric range.

(vi) The characteristics of the interaction and branch mixing of the i-e and e-e instabilities depend on the temperature ratio.

For i-i-e plasmas (with an ion population at rest), the main conclusion is that the ratio of the ion-to-electron cur-

rent decides the instability types that develop in this plasma. In the case of a ''slow'' electron beam, two i-e instabilities develop simultaneously. On the contrary, a ''fast'' electron beam interacts jointly with the two ion populations producing a single i-e instability as in a two-species plasma; simultaneously, a weaker i-i instability develops from the residual interaction between the two ion populations. For an i-i-e plasma, a different form of branch mixing, here between two ion-electron branches, has been found.

Finally, this work has considered plasmas that are planar, homogeneous, and infinite. The stability of the whole structure formed by a strong DL and the two quasineutral plasmas, requires to define adequate boundary conditions and to take into account the perturbation of the DL position and its interaction with the two plasmas. Reference 11 dealt with this problem but restricted to the frequency range of the i-e modes and without Landau resonance effects. Work is in progress to extend that stability study to the e-e instability and to include Landau resonance effects.[21]

ACKNOWLEDGMENT

This research was supported by Ministerio de Educación y Cultura of Spain under Project No. PB97-0574-C04-02.

[1] P. Coakley and N. Hershkowitz, Phys. Fluids **22**, 1171 (1979).
[2] N. Hershkowitz, Space Sci. Rev. **41**, 351 (1985).
[3] M. A. Raadu, Phys. Rep. **178**, 26 (1989).
[4] J. Williams and P. J. Wilbur, J. Spacecr. Rockets **27**, 634 (1990).
[5] E. Ahedo, J. Sanmartín, and M. Martínez-Sánchez, Phys. Fluids B **4**, 3847 (1992).
[6] R. Hubbard and G. Joyce, J. Geophys. Res., [Space Phys.] **84**, 4297 (1979).
[7] G. Vannaroni, M. Dobrowolny, E. Melchioni, F. de Venuto, and R. Giovi, J. Appl. Phys. **71**, 4709 (1992).
[8] D. Hastings and N. Gatsonis, Acta Astron. **17**, 827 (1988).
[9] L. Iess and M. Dobrowolny, Phys. Fluids B **1**, 1880 (1989).
[10] A. Gioulekas and D. Hastings, J. Propul. Power **6**, 559 (1990).
[11] V. Lapuerta and E. Ahedo, Phys. Plasmas **7**, 2693 (2000).
[12] T. E. Stringer, J. Nucl. Energy, Part C **6**, 267 (1964).
[13] S. P. Gary, J. Geophys. Res. **90**, 8213 (1985).
[14] S. P. Gary, Phys. Fluids **30**, 2745 (1987).
[15] H. X. Vu, J. M. Wallace, and B. Bezzerides, Phys. Plasmas **1**, 3542 (1994).
[16] E. A. Williams, R. L. Berger, R. P. Drake, A. M. Rubenchink, B. S. Bauer, D. D. Meyerhofer, A. C. Gaeris, and T. W. Johnston, Phys. Plasmas **2**, 129 (1995).
[17] E. Ahedo and V. Lapuerta, Phys. Plasmas **8**, 3873 (2001).
[18] S. Ichimaru, *Statistical Plasma Physics* (Addison–Wesley, Redwood City, 1992).
[19] V. Lapuerta and E. Ahedo, Phys. Plasmas **9**, 1513 (2002).
[20] A. Krall and A. Trivelpiece, *Principles of Plasma Physics* (San Francisco Press, San Francisco, 1986).
[21] V. Lapuerta and E. Ahedo, in SP-476, *7th Spacecraft Charging Technology Conference* (ESA, Noordwijk, 2001), p. 563.